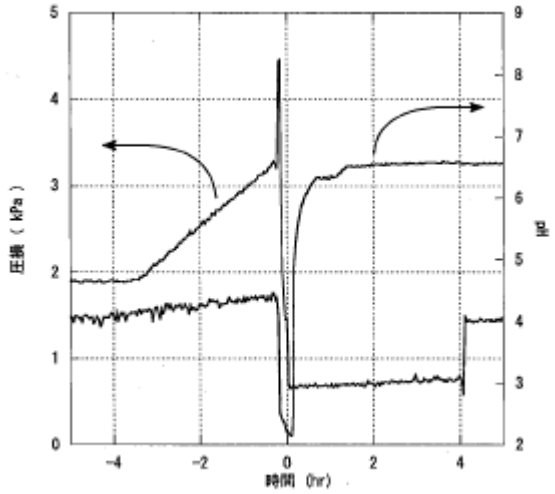

[(left) Pressure loss (kPa) (bottom) Time (h)]
Fig. 4.30 The relation between time, pressure loss, and pH in pressure loss measuring element 1 in ICAN-8.

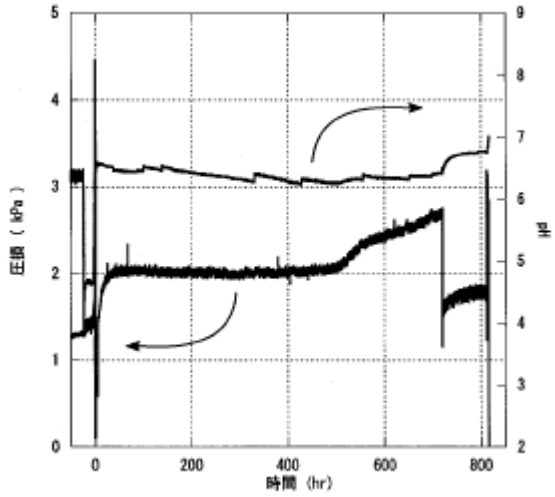

[(left) Pressure loss (kPa) (bottom) Time (h)]
Fig. 4.31 The relation between time, pressure loss, and pH in pressure loss measuring element 1 in ICAN-8.

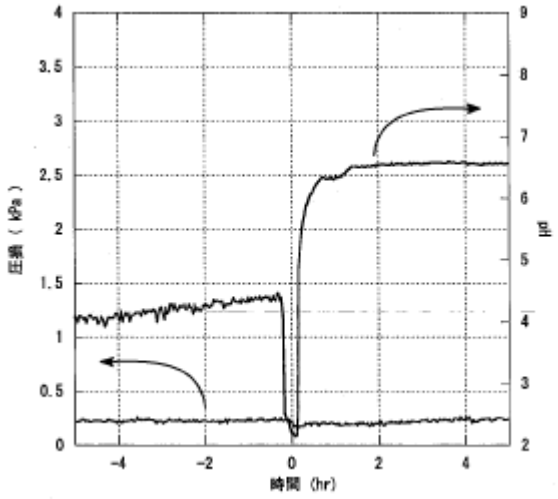

[(left) Pressure loss (kPa) (bottom) Time (h)]
Fig. 4.32 The relation between time, pressure loss, and pH in pressure loss measuring element 2 in ICAN-8.

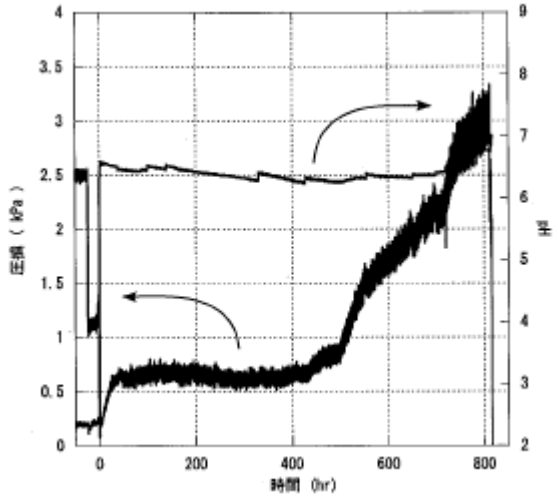

[(left) Pressure loss (kPa) (bottom) Time (h)]
Fig. 4.33 The relation between time, pressure loss, and pH in pressure loss measuring element 2 in ICAN-8.

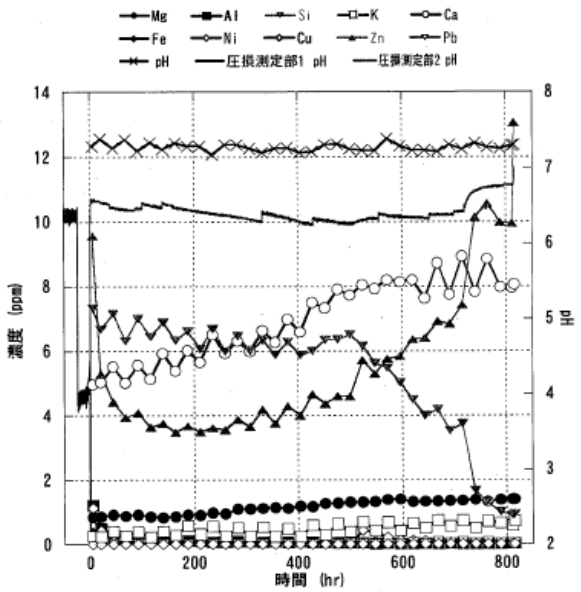

[(top1) --- pH in pressure loss measuring element 1 (top2) --- pH in pressure loss measuring element 2 (left) Concentration (ppm) (bottom) Time (h)]
Fig. 4.34 The relation between the pH of test water samples from the piping and eluting elements in ICAN-8.

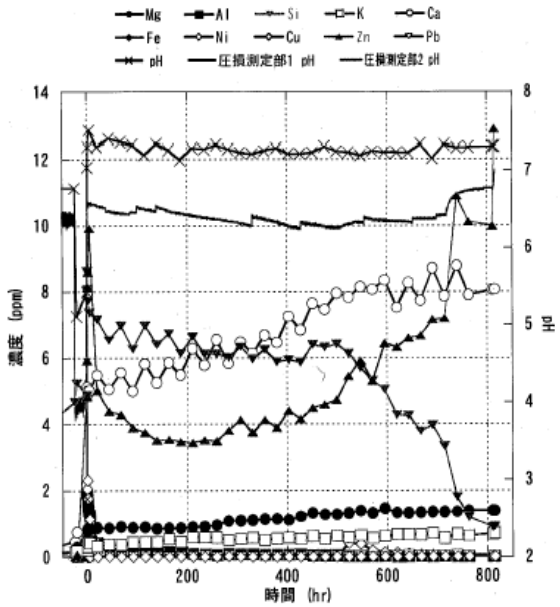

[(top1) --- pH in pressure loss measuring element 1 (top2) --- pH in pressure loss measuring element 2 (left) Concentration (ppm) (bottom) Time (h)]
Fig. 4.35 The relation between the pH of test water sampled from the tanks and eluting elements in ICAN-8.

4.3.1.6 Test water analysis results and solubility of oxides and hydroxides of metal elements

pH-solubility curves for aluminum hydroxide (Gibbsite, $Al(OH)_3$), aluminum hydroxide (amorphous, $Al(OH)_3$), quartz (SiO_2), amorphous silica (SiO_2), iron oxide (hematite, Fe_2O_3), copper oxide (CuO), and zinc oxide (ZnO) employing thermodynamics data are recorded in an appendix. In integrated chemical effect assessment tests conducted thus far under PWR conditions, pH regulating agents in the form of sodium hydroxide (ICAN-1, 2, 3, 7) sodium tetraborate (ICAN-4), and hydrazine (ICAN-5, 8) have been employed. The approximate pH values when these various regulating agents are employed are pH = 10 for sodium hydroxide, pH = 8.3 for sodium tetraborate, and pH = 7.2 for hydrazine. A test (ICAN-6) under BWR conditions, in which no pH regulating agent was employed, has also been conducted. The approximate pH value in this test was pH = 5.7.

The analytic values for Al were, for hydrazine (pH = 7.2): 0.01 to 0.5 ppm, for sodium tetraborate (pH = 8.3): 4.5 ppm, and for sodium hydroxide (pH=10): 2 to 6 ppm. The solubility of Al, assuming Gibbsite as solid phase, for pH levels of 7.2, 8.3, and 10 is 0.0003, 0.003, and 0.17 ppm, respectively (Fig. A.1). The solubility of Al, assuming amorphous aluminum hydroxide as solid phase, for pH levels of 7.2, 8.3, and 10 is 0.24, 2.9, and 145, respectively (Fig. A.2). The analytic values are close to the values assumed for the presence of Gibbsite, but are higher than the calculated values. Al has not been placed in a liquid phase portion under BWR conditions.

The analytic values for Si were, under BWR conditions (pH = 5.7): 2 to 2.5 ppm, for hydrazine (pH = 7.2): 1 to 15 ppm, for sodium tetraborate (pH = 8.3): 10 to 15 ppm, and for sodium hydroxide (pH = 10): 10 to 15 ppm. The solubility of Si, assuming quartz as solid phase, for pH levels of 5.7, 7.2, 8.3, and 10, is 2.8, 2.8, 2.9, and 7.2 ppm, respectively (Fig. A.3). The solubility of Al, assuming amorphous silica as solid phase, for pH levels of 5.7, 7.2, 8.3, and 10 is 54, 54, 56, and 137 ppm, respectively (Fig. A.4). The analytic values are close to the values assumed for the presence of quartz, but are higher than the calculated values.

With the exception of the test under BWR conditions, the concentration of iron was 0 ppm, which is a suitable result when the solubility of hematite is considered (Fig. A.5). In the BWR test, the concentration of iron reached 40 ppm at the end of the test. This could not be explained from the dissolution of hematite. The dissolution of such a high concentration of iron was attributed to the high solubility of iron oxide due to the presence of chloride ions (Cl^-).

The analytic values for copper were, for hydrazine (pH 7.2): 0 to 0.01 ppm, for sodium tetraborate (pH = 8.3): about 0.1 ppm, and for sodium hydroxide (pH = 10): about 0.8 ppm. The solubility of copper oxide, for pH levels of 7.2, 8.3, and 10, is 0.01, 0.0002, and 0.0007 ppm, respectively (Fig. A.6). The analytic value was greater than the calculated value, but qualitatively matched from the perspective of low solubility in the alkaline range. The solubility at a pH of 5.7 under BWR conditions was about 10 ppm. However, in ICAN-6, since no copper was placed in the liquid phase portion, the actual concentration of copper in the test water was about 1 ppm.

The analytic value of zinc was, under BWR conditions (pH = 5.7): 7 to 15 ppm, and for hydrazine (pH = 7.2): 4 to 13 ppm. Zinc steel was only placed in the liquid phase portion in ICAN-6 and ICAN-8. In the other tests, the analytic value of zinc could not be compared to the calculated value. The solubility of zinc oxide at pH levels of 5.7 and 7.2 is 28,000 and 87 ppm, respectively (Fig. A.7). The analytic value under BWR conditions was much smaller than the calculated value, which was probably due to the fact that only a single test piece of zinc steel was placed in the liquid phase portion. The solubility of zinc oxide at pH levels of 8.3 and 10 was 0.33 and 0.01 ppm, respectively.

The analytic values of Al, Si, and Cu matched the calculated values rather well when the fact that the quantitative addition was 0.001 or 0.002 ppm is considered. When just oxides were considered, Fe did not match the calculated quantity; it was necessary to take the anions that were present into account. The solubility of Zn increases in the acid range, but in the test under BWR conditions, the quantity of Zn decreased and was thought to reach equilibrium.

/105

In the calculation of the solubility of Cu and Zn, the solubility of copper oxide and zinc oxide at pH levels varying from 4 to 10 is extremely low. Thus, large amounts

of copper oxide and zinc oxide were thought to precipitate out (Fig. A.6, A.7). Although hydroxides of Al precipitate out under similar conditions, the degree to which they do so is less than that of copper and zinc (Fig. A.1).

/106

4.3.2. The appearance and change in weight of test coupons

4.3.2.1 ICAN-4

Fig. 4.36 and 4.37 are photographs showing the appearance of the metal test pieces placed in the gas phase portion. Red rust thought to be FeOOH or Fe_2O_3 formed on the carbon steel (Fig. 4.36). A white corrosion product thought to be $Al(OH)_3$ was observed on the aluminum (Fig. 4.37). Figs. 4.38 to 4.40 are photographs showing the appearance of the metal test pieces placed in the liquid phase portion. Reddish brown rust thought to be FeOOH or Fe_2O_3 formed on the carbon steel to a greater degree than in the gas phase portion (Fig. 4.38). The aluminum in the liquid phase portion was much more corroded than the aluminum in the gas phase portion (Fig. 4.39). Although exposure or the like of the base (carbon steel) due to corrosion was not seen in painted sample strips, a white corrosion product thought to be ZnO formed (Fig. 4.40). Table 4.25 and Fig. 4.41 show the change in weight per piece of metal coupon before and after the test. A large amount of powdery substance adhered to the coupons; the change in weight was measured after the removal of this substance. The weight of all the metal test pieces increased due to oxidation. The corrosion (oxidation) of carbon steel and paint material in the liquid phase portion was found to be particularly severe.

(a) Before test

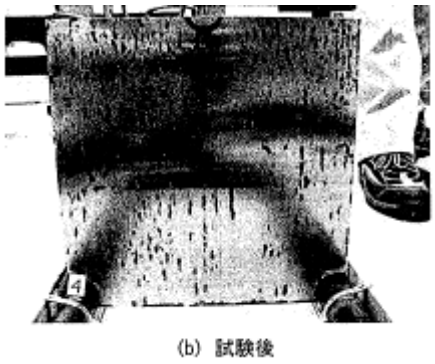

(b) After test

Fig. 4.36 The appearance before and after the test of carbon steel that was placed in the gas phase portion in an integrated chemical effect assessment test (ICAN-4)

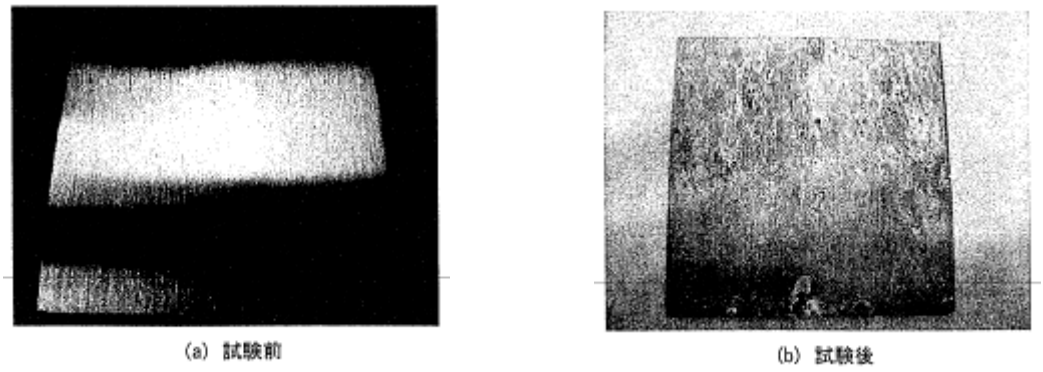

(a) Before test (b) After test

Fig. 4.37 The appearance before and after the test of aluminum that was placed in the gas phase portion in an integrated chemical effect assessment test (ICAN-4)

/107

(a) 試験前

(b) 試験後

(a) Before test (b) After test

Fig. 4.38 The appearance before and after the test of carbon steel that was placed in the liquid phase portion in an integrated chemical effect assessment test (ICAN-4)

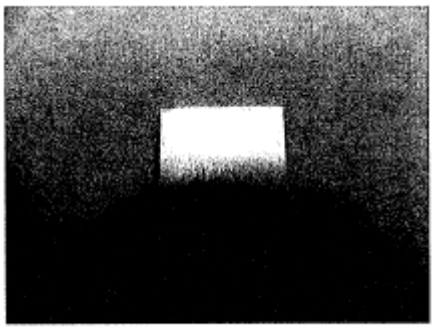

(a) 試験前

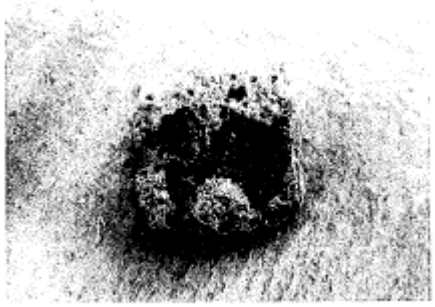

(b) 試験後

(a) Before test (b) After test

Fig. 4.39 The appearance before and after the test of aluminum that was placed in the liquid phase portion in an integrated chemical effect assessment test (ICAN-4)

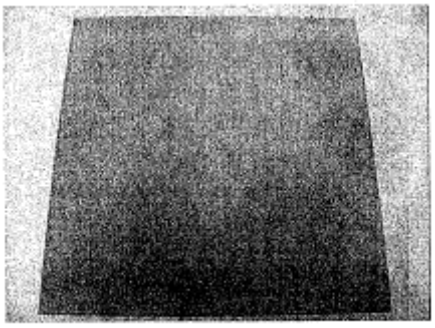

(a) 試験前

(b) 試験後

(a) Before test (b) After test

Fig. 4.40 The appearance before and after the test of paint that was placed in the liquid phase portion in an integrated chemical effect assessment test (ICAN-4)

Table 4.25 The change in weight (g) per coupon

Gas phase portion		Liquid phase portion		
Carbon steel	Aluminum	Carbon steel	Aluminum	Paint
0.31	0.05	6.60	0.05	11.40

/108

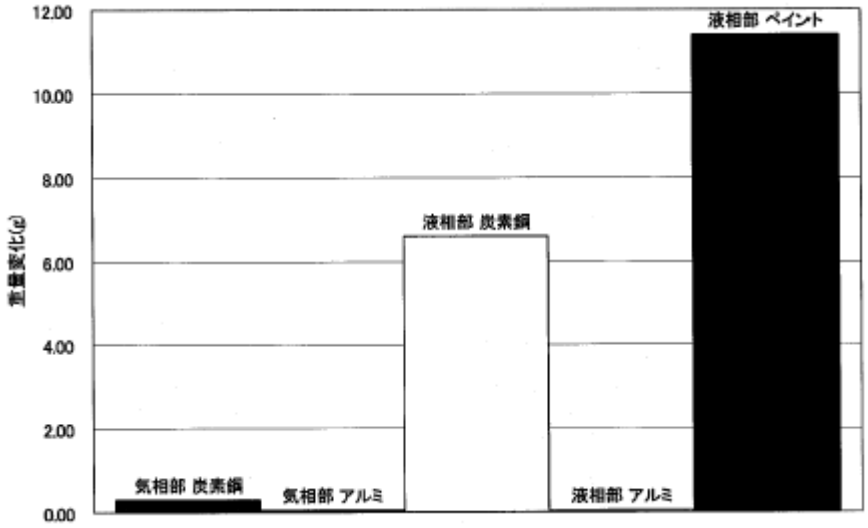

[(left vertical) Weight change (g) (bottom left) Carbon steel in gas phase portion (bottom second) Aluminum in gas phase portion (bottom third) Carbon steel in liquid phase portion (bottom fourth) Aluminum in liquid phase portion (bottom right) Paint in liquid phase portion]

Fig. 4.41 Change in weight of metal test pieces in integrated chemical effect assessment test (ICAN-4).

4.3.2.2 ICAN-5

Figs. 4.42 to 4.44 are photographs showing the appearance of metal test pieces placed in the gas phase portion. A tea-brown rust formed on the carbon steel (Fig. 4.42). This was thought to be FeOOH or Fe_2O_3. Black CuO was observed on the copper sheet (Fig. 4.43). White Al_2O_3 adhered to the aluminum, but the degree of corrosion was not great (Fig. 4.44). Figs. 4.45 to 4.48 are photographs showing the appearance of metal test pieces placed in the liquid gas portion. The carbon steel was covered by reddish-brown rust thought to be FeOOH or Fe_2O_3 (Fig. 4.45). The red rust was readily removed by washing with water. The copper was covered with black CuO (Fig. 4.46). Tea-brown and white corrosion products adhered to the surface of the aluminum (Fig. 4.47). Reddish-brown iron rust adhered to the paint sample strip, but corrosion of the paint itself was not marked (Fig. 4.48). Table 4.26 and Fig. 4.49 show the change in weight per coupon before and after the test. The weight of the coupons in the gas phase portion increased due to oxidation, while the weight of the coupons in the liquid phase portion was reduced by corrosion. In particular, the weight of the carbon steel in the liquid phase portion decreased more than 18 g; the corrosion was more severe than when a pH regulating agent in the form of sodium hydroxide or sodium tetraborate was employed.

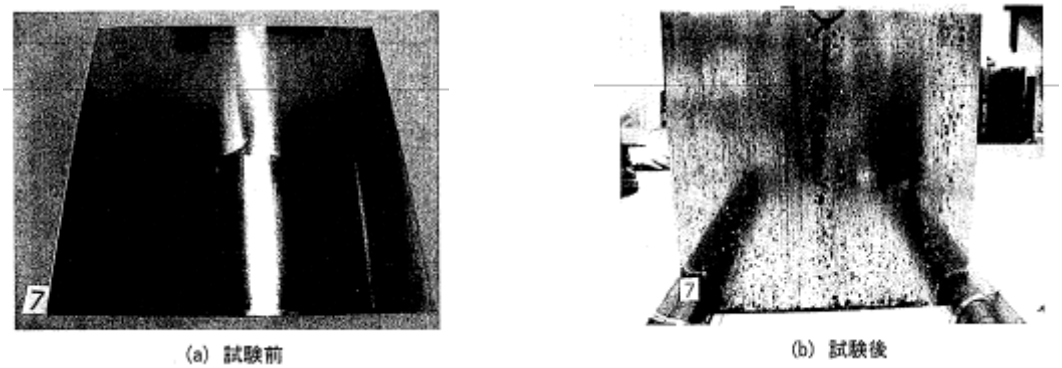

(a) Before test (b) After test

Fig. 4.42 The appearance before and after the test of carbon steel that was placed in the gas phase portion in an integrated chemical effect assessment test (ICAN-5)

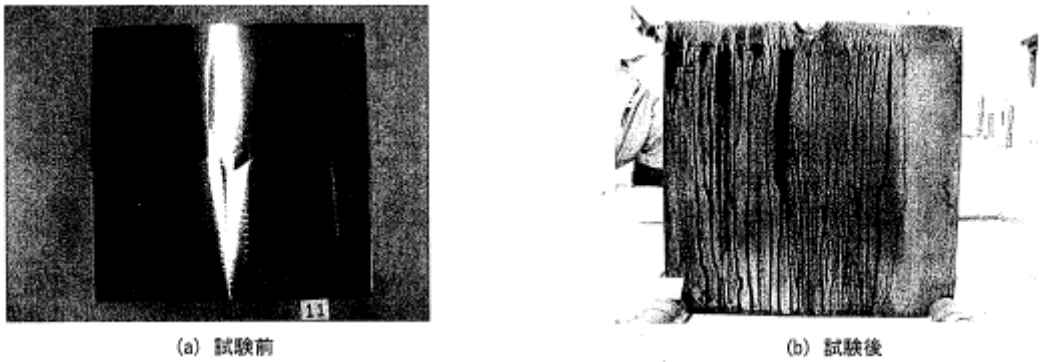

(a) Before test (b) After test

Fig. 4.43 The appearance before and after the test of copper that was placed in the gas phase portion in an integrated chemical effect assessment test (ICAN-5)

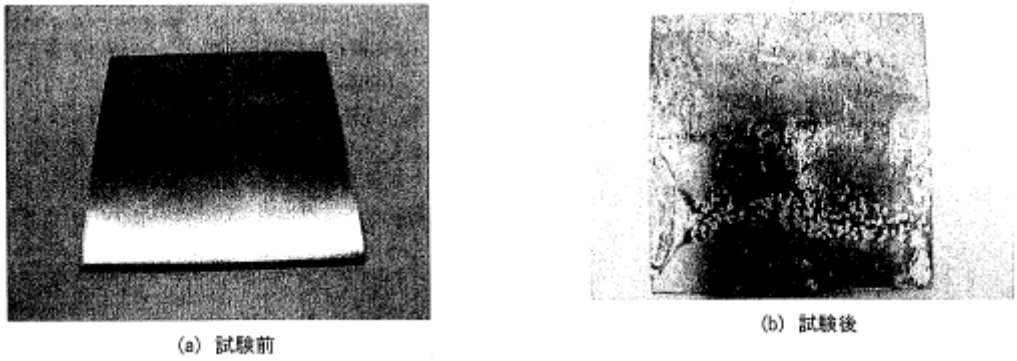

(a) Before test (b) After test

Fig. 4.44 The appearance before and after the test of aluminum that was placed in the gas phase portion in an integrated chemical effect assessment test (ICAN-5)

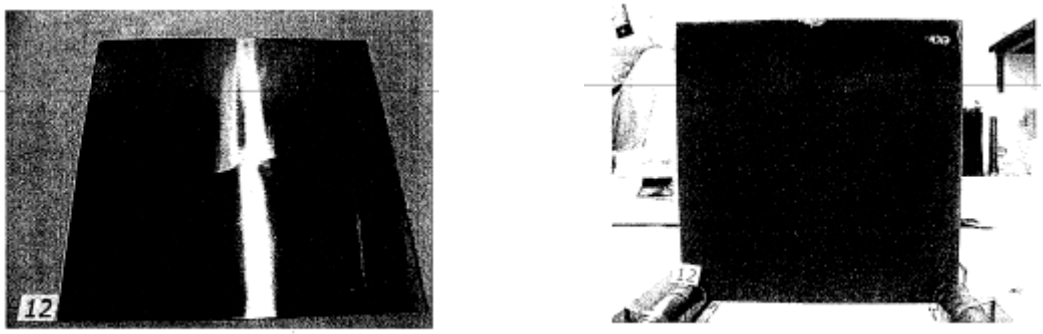

(a) Before test (b) After test

Fig. 4.45 The appearance before and after the test of carbon steel that was placed in the liquid phase portion in an integrated chemical effect assessment test (ICAN-5)

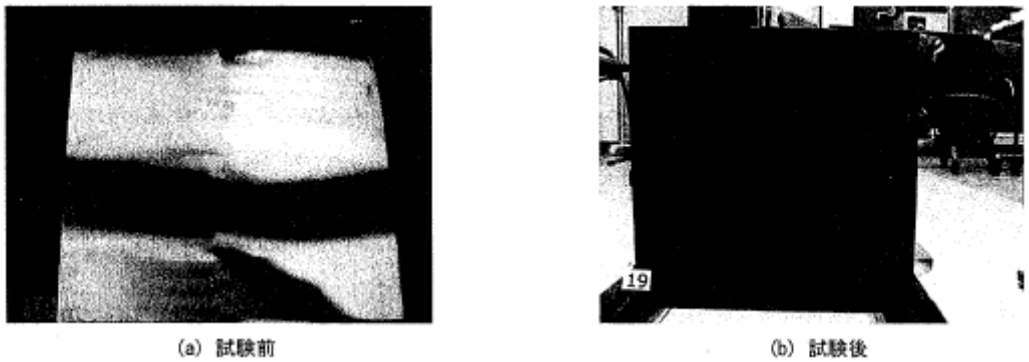

(a) Before test (b) After test

Fig. 4.46 The appearance before and after the test of copper that was placed in the liquid phase portion in an integrated chemical effect assessment test (ICAN-5)

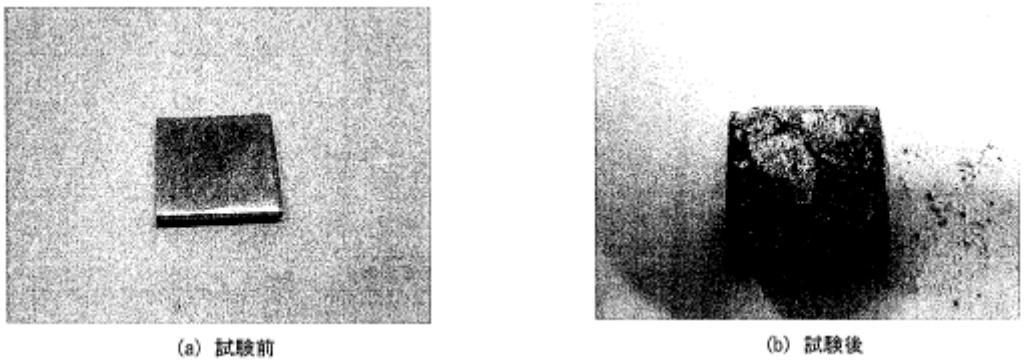

(a) Before test (b) After test

Fig. 4.47 The appearance before and after the test of aluminum that was placed in the liquid phase portion in an integrated chemical effect assessment test (ICAN-5)

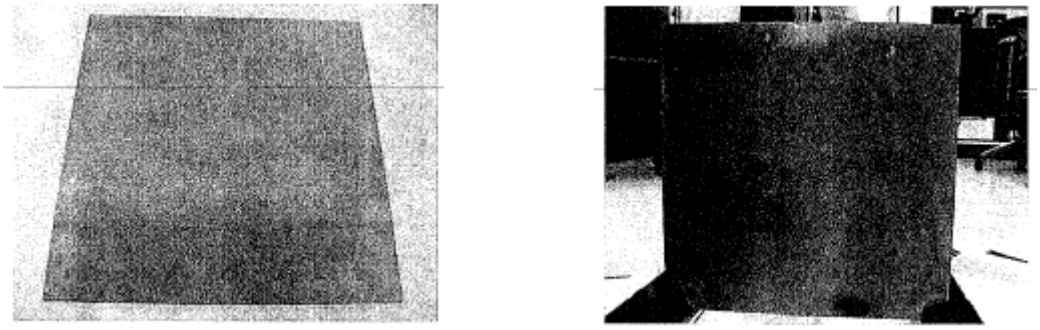

(a) Before test (b) After test

Fig. 4.48 The appearance before and after the test of paint that was placed in the liquid phase portion in an integrated chemical effect assessment test (ICAN-5)

Table 4.26 The change in weight (g) per coupon

Carbon steel	Copper	Aluminum	Carbon steel	Copper	Aluminum	Paint
-0.04	0.16	0.05	-18.53	-0.10	-0.67	-1.00

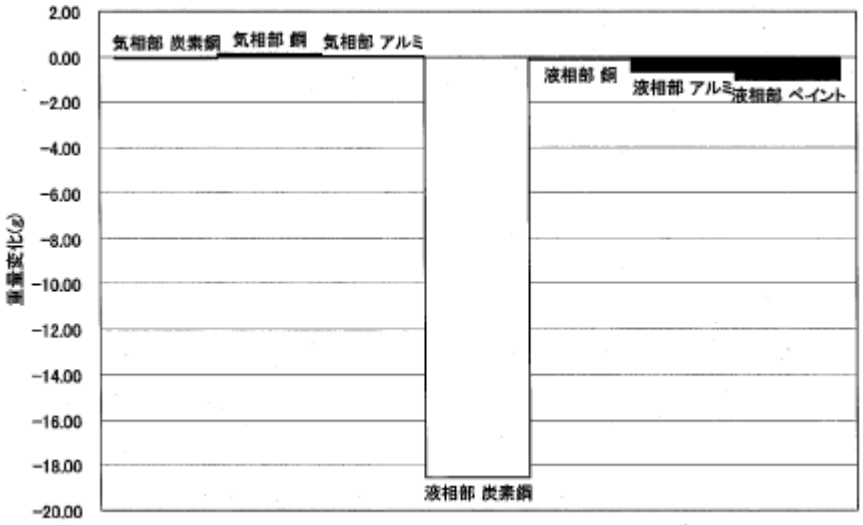

[(left vertical) Weight change (g) (top left, 3 items) Carbon steel in gas phase portion, Copper in gas phase portion, Aluminum in gas phase portion (bottom) Carbon steel in liquid phase portion (top right, 3 items) Copper in liquid phase portion, Aluminum in liquid phase portion, Paint in liquid phase portion]

Fig. 4.49 Change in weight of carbon steel and copper in integrated chemical effect assessment test (ICAN-5)

4.3.2.3 ICAN-6

Figs. 4.50 to 4.56 are photographs showing the appearance of metal test pieces placed in the gas phase portion. Tea-brown rust, thought to be FeOOH or Fe_2O_3, formed on the carbon steel (Fig. 4.50). Black CuO was observed on the copper sheet (Fig. 4.51). White ZnO_2 adhered to the zinc steel (Fig. 4.53). Figs. 4.54 to 4.56 are photographs showing the appearance of metal test pieces (coupons) placed in the liquid phase portion. The carbon steel was covered by reddish-brown rust thought to be FeOOH or Fe_2O_3 (Fig. 4.54).

Brown iron rust adhered to the zinc steel and paint Figs. 4.55 and 4.56). Table 4.27 and Fig. 4.57 show changes in weight per coupon before and after the test. The weight of coupons in the gas phase portion increased due to oxidation, and the weight of coupons in the liquid phase portion decreased due to corrosion, with the exception of paint. In particular, the weight of the carbon steel in the liquid phase portion decreased 59 g, indicating that the acidic test water, which contained hydrochloric acid, caused severe corrosion of iron.

(a) Before test (b) After test

Fig. 4.50 The appearance before and after the test of carbon steel that was placed in the gas phase portion in an integrated chemical effect assessment test (ICAN-6)

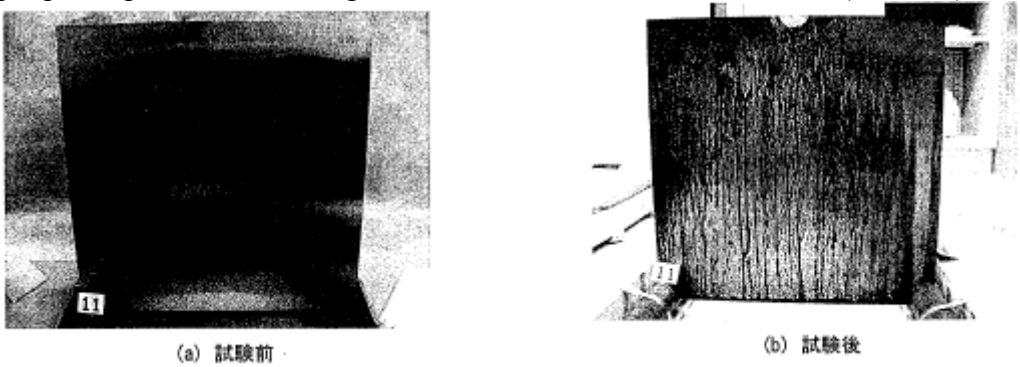

(a) Before test (b) After test

Fig. 4.51 The appearance before and after the test of copper that was placed in the gas phase portion in an integrated chemical effect assessment test (ICAN-6)

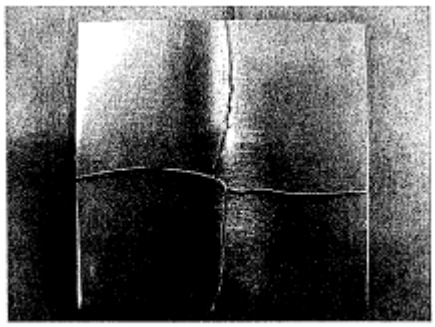

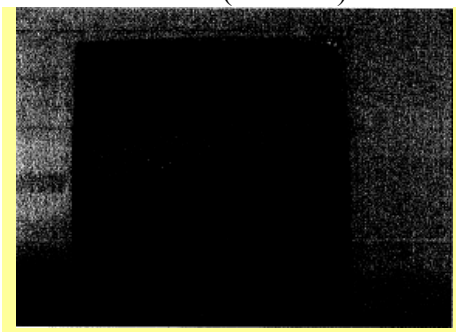

(a) Before test (b) After test

Fig. 4.52 The appearance before and after the test of aluminum that was placed in the gas phase portion in an integrated chemical effect assessment test (ICAN-6)

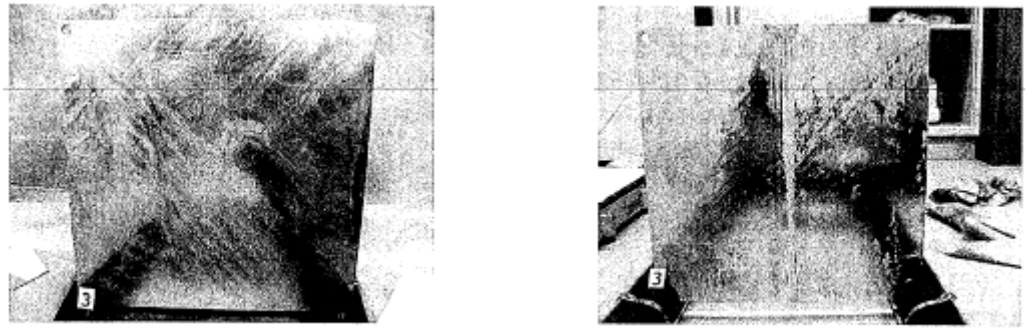

(a) 試験前　(b) 試験後

(a) Before test　(b) After test

Fig. 4.53 The appearance before and after the test of zinc steel that was placed in the gas phase portion in an integrated chemical effect assessment test (ICAN-6)

(a) 試験前　(b) 試験後

(a) Before test　(b) After test

Fig. 4.54 The appearance before and after the test of carbon steel that was placed in the liquid phase portion in an integrated chemical effect assessment test (ICAN-6)

(a) 試験前　(b) 試験後

(a) Before test　(b) After test

Fig. 4.55 The appearance before and after the test of zinc steel that was placed in the liquid phase portion in an integrated chemical effect assessment test (ICAN-6)

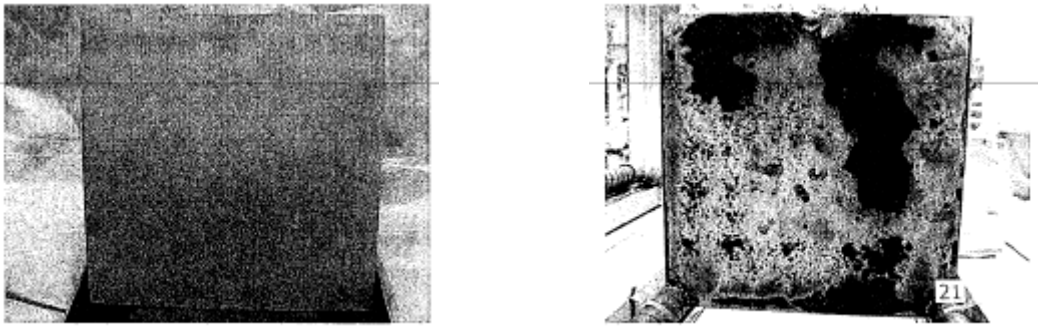

(a) Before test (b) After test

Fig. 4.56 The appearance before and after the test of paint that was placed in the liquid phase portion in an integrated chemical effect assessment test (ICAN-6)

Table 4.27 The change in weight (g) per coupon

Gas phase portion				Liquid phase portion			
Carbon steel	Copper	Aluminum	Zinc steel	Carbon steel	Aluminum	Zinc steel	Paint
2.90	0.05	0.05	0.52	-59.00	-0.67	-1.70	3.30

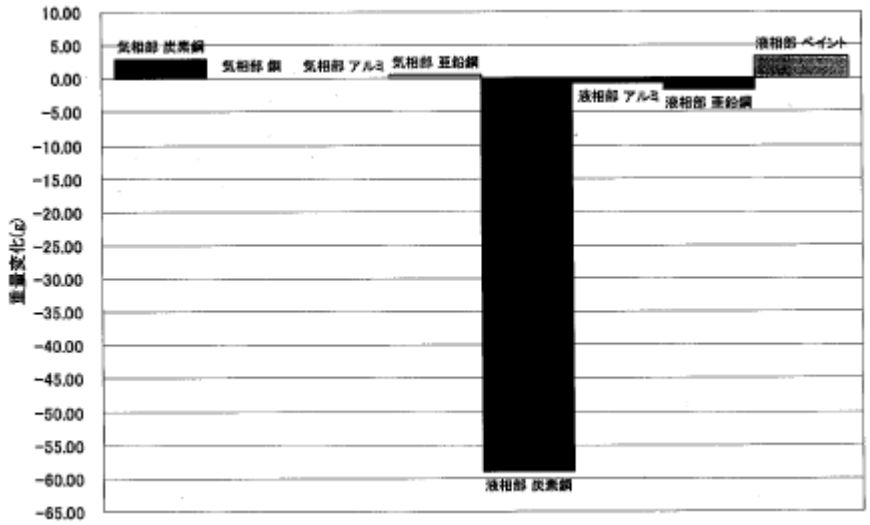

[(left vertical) Weight change (g) (top left, 4 items) Carbon steel in gas phase portion, Copper in gas phase portion, Aluminum in gas phase portion Zinc steel in gas phase portion (bottom) Carbon steel in liquid phase portion (top right, 3 items) Aluminum in liquid phase portion, Zinc steel in liquid phase portion, Paint in liquid phase portion]

Fig. 4.57 Change in weight of carbon steel and copper in integrated chemical effect assessment test (ICAN-6)

4.3.2.4 ICAN 7

Figs. 4.58 to 4.60 are photographs showing the appearance of metal test pieces placed in the gas phase portion. A tea-brown rust thought to be FeOOH or Fe_2O_3 formed on the carbon steel (4.58). Black CuO formed on the copper sheet (Fig. 4.59). Figs. 4.61 to 4.64 are photographs showing the appearance of metal test pieces (coupons) placed in the liquid phase portion. A white corrosion product adhered to the carbon steel and copper (Fig. 4.61 and 4.62). The aluminum appeared black, but there was little corrosion (Fig. 4.63). The paint also appeared black, but underwent little corrosion (Fig. 4.64). Table 4.28 and Fig. 4.65 show the change in weight per coupon before and after the test. There was little change in weight of coupons in the liquid phase portion. When a pH regulating agent in the form of sodium hydroxide was employed, little corrosion of metal was found to occur.

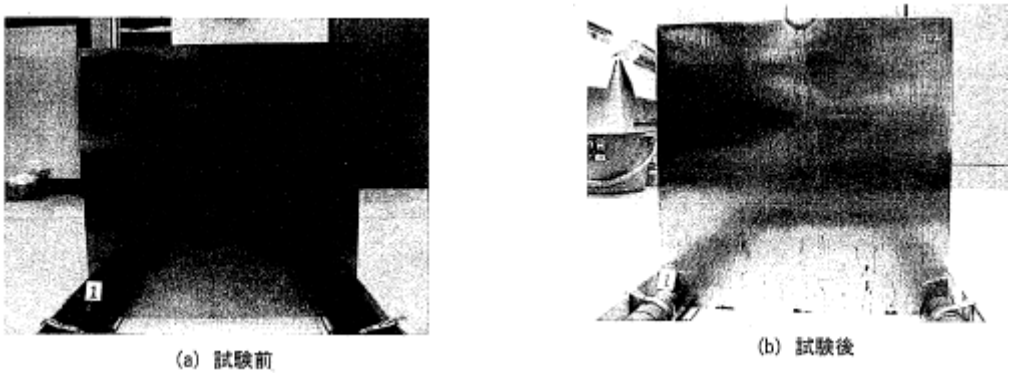

(a) Before test (b) After test

Fig. 4.58 The appearance before and after the test of carbon steel that was placed in the gas phase portion in an integrated chemical effect assessment test (ICAN-7)

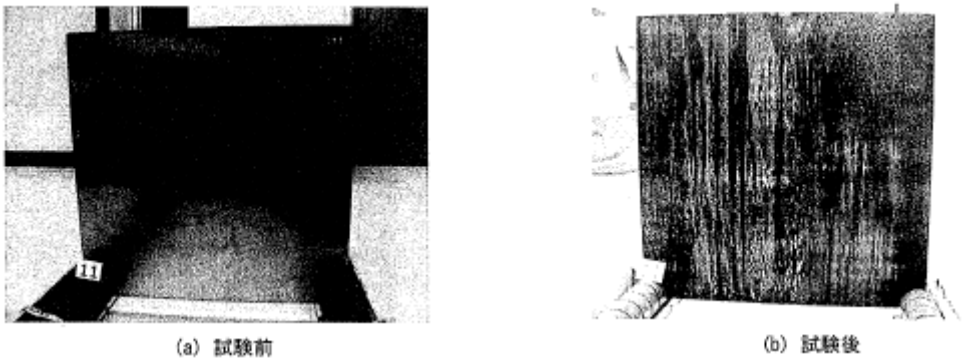

(a) Before test (b) After test

Fig. 4.59 The appearance before and after the test of copper that was placed in the gas phase portion in an integrated chemical effect assessment test (ICAN-7)

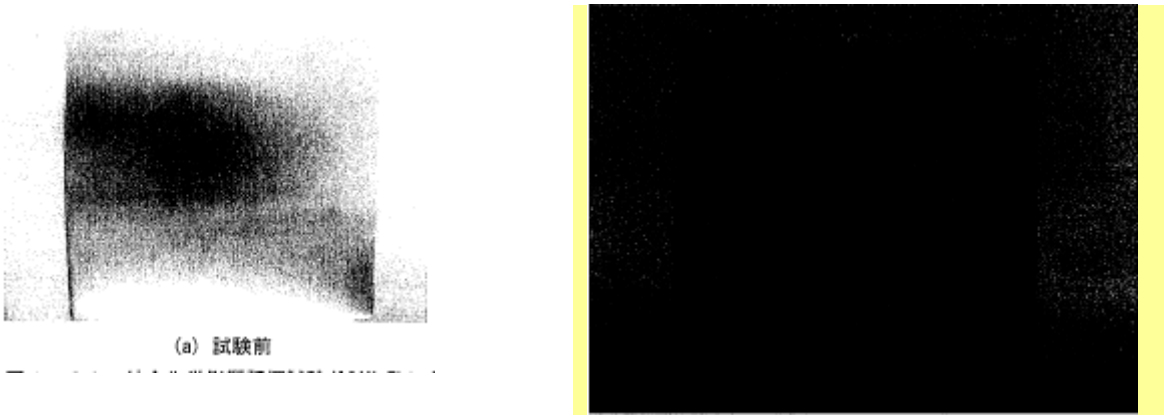

(a) Before test (b) After test

Fig. 4.60 The appearance before and after the test of aluminum that was placed in the gas phase portion in an integrated chemical effect assessment test (ICAN-7)

/116

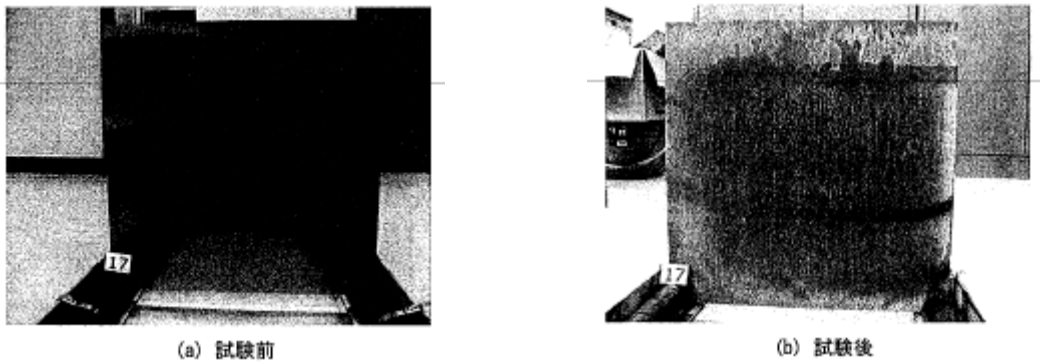

(a) Before test (b) After test

Fig. 4.61 The appearance before and after the test of carbon steel that was placed in the liquid phase portion in an integrated chemical effect assessment test (ICAN-7)

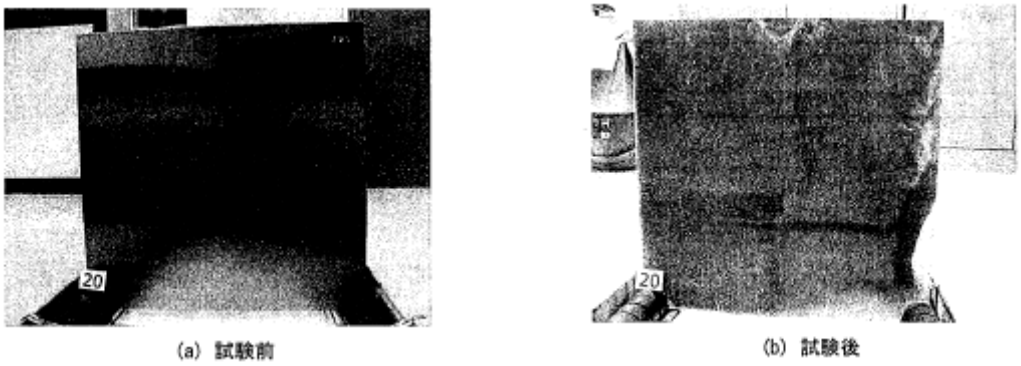

(a) Before test (b) After test

Fig. 4.62 The appearance before and after the test of copper that was placed in the liquid phase portion in an integrated chemical effect assessment test (ICAN-7)

(a) Before test (b) After test

Fig. 4.63 The appearance before and after the test of aluminum that was placed in the liquid phase portion in an integrated chemical effect assessment test (ICAN-7)

/117

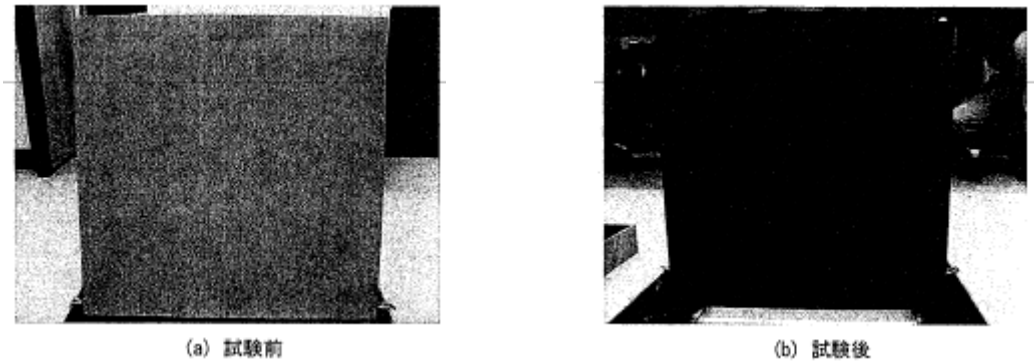

(a) Before test (b) After test

Fig. 4.64 The appearance before and after the test of paint that was placed in the liquid phase portion in an integrated chemical effect assessment test (ICAN-7)

Table 4.28 The change in weight (g) per coupon

Gas phase portion			Liquid phase portion			
Carbon steel	Copper	Aluminum	Carbon steel	Copper	Aluminum	Paint
-0.09	0.14	-0.11	-0.63	-0.97	-0.44	0.60

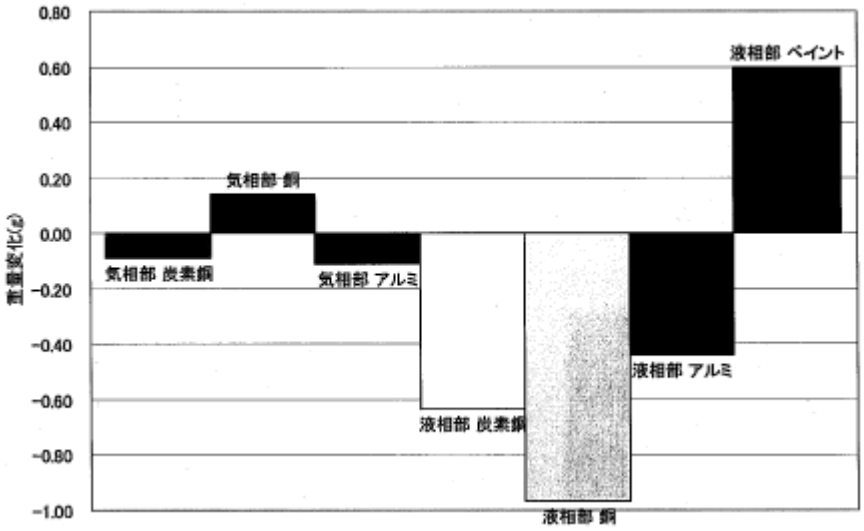

[(left vertical) Weight change (g) (inside graph, from left) Carbon steel in gas phase portion, Copper in gas phase portion, Aluminum in gas phase portion, Carbon steel in liquid phase portion, Copper in liquid phase portion, Aluminum in liquid phase portion, Paint in liquid phase portion]
Fig. 4.65 Change in weight of carbon steel and copper in integrated chemical effect assessment test (ICAN-7)

4.3.2.5 ICAN-8

Figs. 4.66 to 4.69 are photographs showing the appearance of metal test pieces placed in the gas phase portion. Tea-brown rust thought to be FeOOH or FeO_3 formed on the carbon steel (Fig. 4.66). Black CuO was found on the copper sheet (Fig. 4.67). White Al_2O_3 adhered to the aluminum, but the degree of corrosion was not great (Fig. 4.68). White ZnO_2 adhered to the zinc steel (Fig. 4.69). Figs. 4.70 to 4.74 are photographs showing the appearance of test metal pieces (coupons) placed in the liquid phase portion. Reddish-brown rust lumps, thought to be FeOOH or Fe_2O_3, formed on the carbon steel (Fig. 4.70). This was in contrast to the rust in ICAN-5, also a test of water quality, which adhered uniformly. Bluish-white $Cu(OH)_2$ adhered to the copper (Fig. 4.71). $Cu(OH)_2$ is said to dehydrate at 60 to 80ºC and convert to CuO. However, in ICAN-8, in contrast to ICAN-5, a portion remained as $Cu(OH)_2$. White corrosion product adhered to the surface of the aluminum (Fig. 4.72). The zinc steel underwent severe corrosion, and was covered in white ZnO (Fig. 4.73). A white corrosion product was also observed on paint test pieces (Fig. 4.74). Tables 4.29 and 4.75 show the changes in weight per coupon before and after the test. With the exception of aluminum, the coupons placed in the gas phase portion increased in weight due to oxidation. With the exception of copper, the coupons placed in the liquid phase portion decreased in weight due to corrosion. In particular, the weight of the carbon steel and the zinc steel in the liquid phase portion decreased by 9.5 g and 12.5 g, respectively. This was more severe corrosion than when a pH regulating agent in the form of sodium hydroxide or sodium tetraborate was employed.

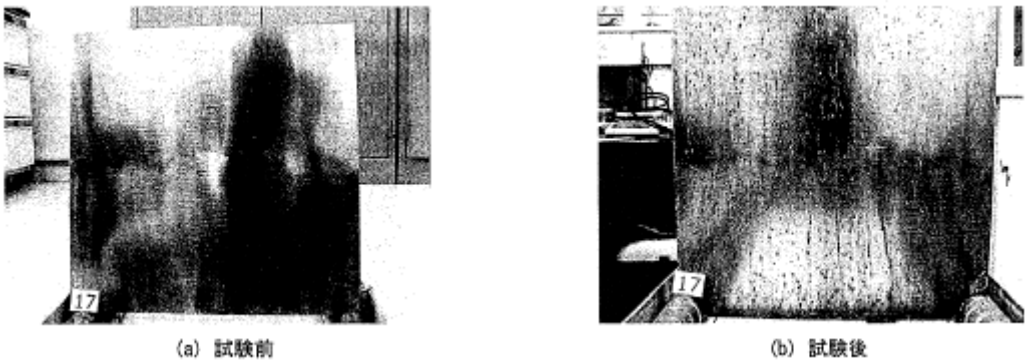

(a) Before test (b) After test

Fig. 4.66 The appearance before and after the test of carbon steel that was placed in the

gas phase portion in an integrated chemical effect assessment test (ICAN-8)

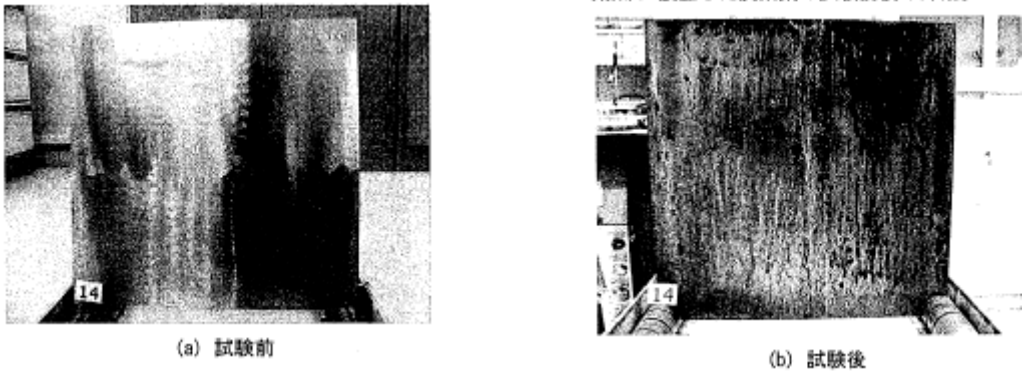

(a) Before test (b) After test

Fig. 4.67 The appearance before and after the test of copper that was placed in the gas phase portion in an integrated chemical effect assessment test (ICAN-8)

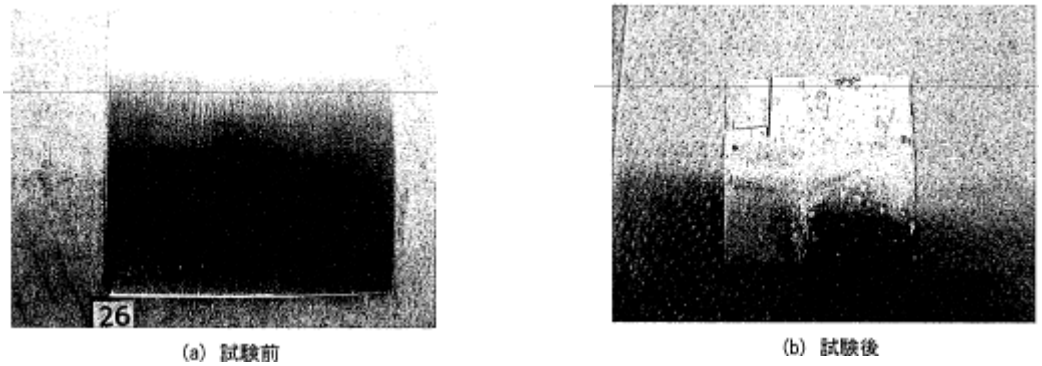

(a) Before test (b) After test

Fig. 4.68 The appearance before and after the test of aluminum that was placed in the gas phase portion in an integrated chemical effect assessment test (ICAN-8)

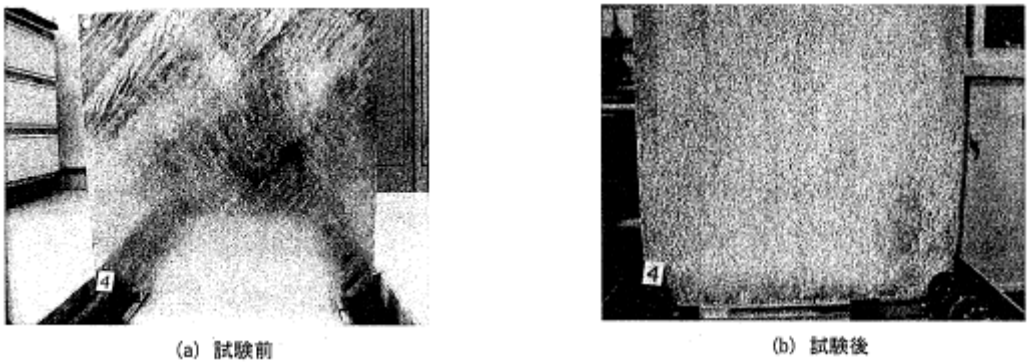

(a) Before test (b) After test

Fig. 4.69 The appearance before and after the test of zinc steel that was placed in the gas phase portion in an integrated chemical effect assessment test (ICAN-8)

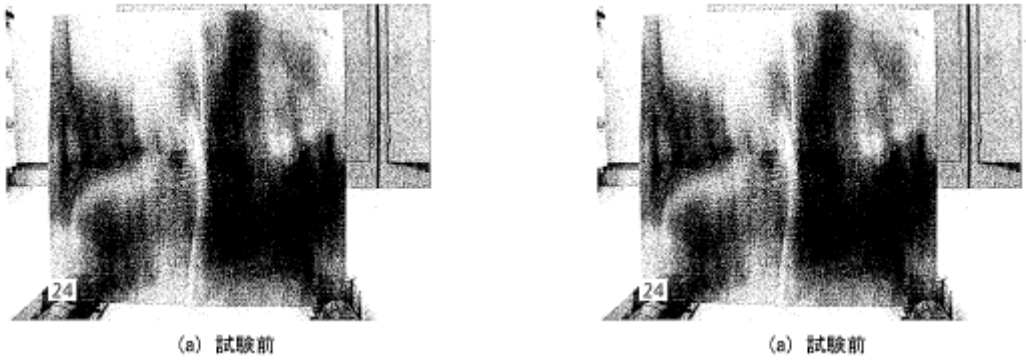

(a) Before test (b) After test

Fig. 4.70 The appearance before and after the test of carbon steel that was placed in the liquid phase portion in an integrated chemical effect assessment test (ICAN-8)

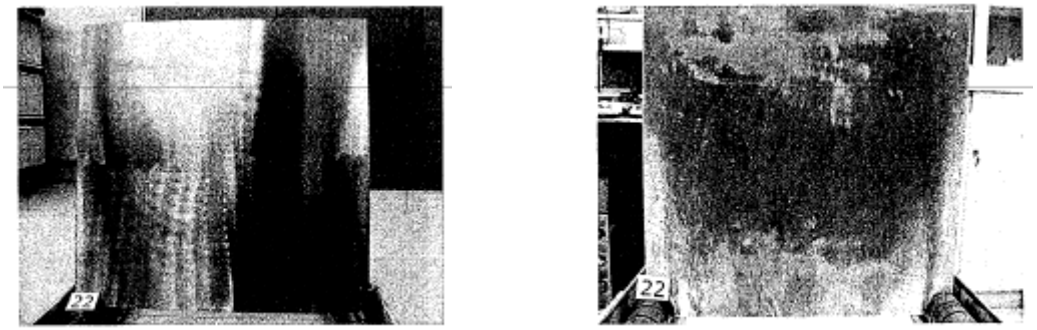

(a) 試験前　(b) 試験後

(a) Before test　(b) After test

Fig. 4.71 The appearance before and after the test of copper that was placed in the liquid phase portion in an integrated chemical effect assessment test (ICAN-8)

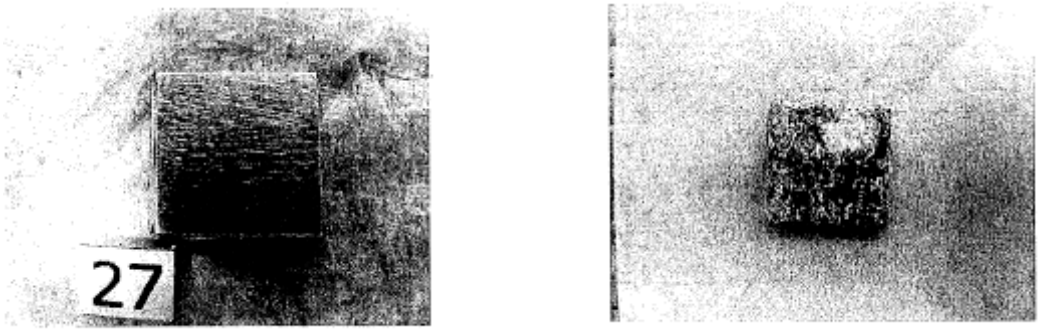

(a) 試験前　(b) 試験後

(a) Before test　(b) After test

Fig. 4.72 The appearance before and after the test of aluminum that was placed in the liquid phase portion in an integrated chemical effect assessment test (ICAN-8)

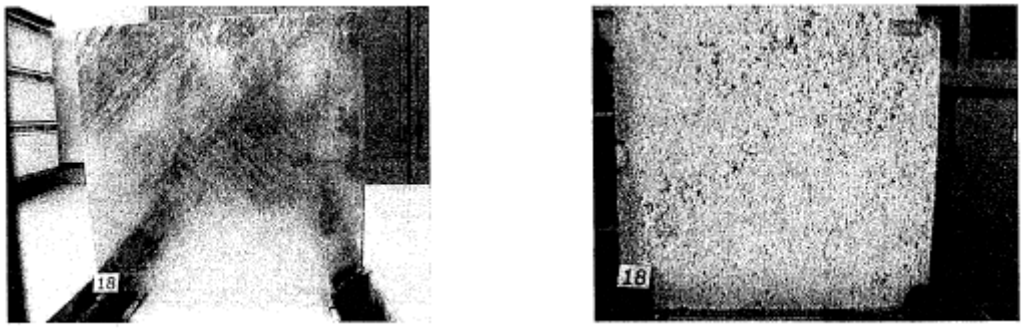

(a) 試験前　(b) 試験後

(a) Before test　(b) After test

Fig. 4.73 The appearance before and after the test of zinc steel that was placed in the liquid phase portion in an integrated chemical effect assessment test (ICAN-8)

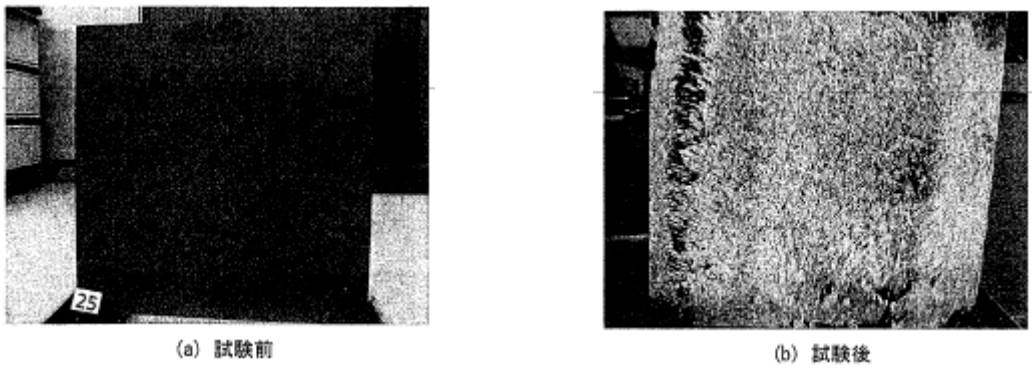

(a) Before test (b) After test

Fig. 4.74 The appearance before and after the test of paint that was placed in the liquid phase portion in an integrated chemical effect assessment test (ICAN-8)

Table 4.29 The change in weight (g) per coupon

Gas phase portion				Liquid phase portion				
Carbon steel	Copper	Aluminum	Zinc steel	Carbon steel	Copper	Aluminum	Zinc steel	Paint
0.35	0.20	-0.02	2.68	-9.50	0.47	-0.02	-12.47	0.30

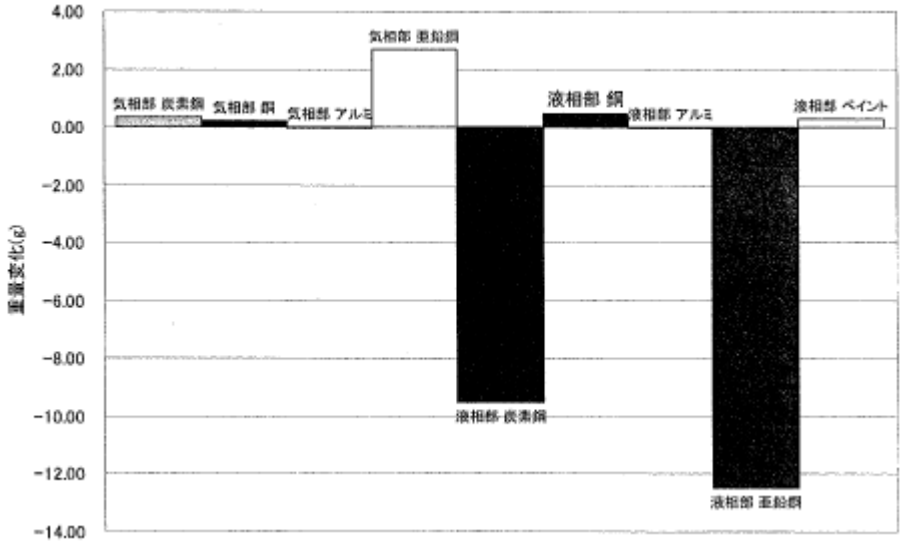

[(left vertical) Weight change (g) (inside graph, from left) Carbon steel in gas phase portion, Copper in gas phase portion, Aluminum in gas phase portion, Zinc steel in gas phase portion, Carbon steel in liquid phase portion, Copper in liquid phase portion, Aluminum in liquid phase portion, Zinc steel in liquid phase portion, Paint in liquid phase portion]

Fig. 4.75 Change in weight of carbon steel and copper in integrated chemical effect assessment test (ICAN-8)

/122

5. Conclusion

Corrosion tests were conducted on insulating materials in sodium tetraborate solution, hydrazine solution, and a solution of hydrochloric acid added to pure water under BWR conditions with the objective of obtaining basic data to examine integrated chemical effect test results. For rock wool insulating material, the concentration of elements that dissolved increased with the pH. In the calcium silicate corrosion test, the pH of the hydrochloric acid solution rose to 9.2 in the three hours following the start of the test, making this the test in which the highest pH was reached in the test solution. For calcium silicate insulating material, the concentration of dissolving elements decreased as the pH increased.

In pressure loss tests, the status of debris and the effects on pressure loss on simulated colloids of corrosion products were examined. Colloid particles had a greater tendency to increase the pressure loss than calcium silicate. In particular, iron hydroxide and aluminum hydroxide had a greater tendency to increase the pressure loss than copper oxide. In a test employing sodium tetraborate as a pH regulating agent, the pressure loss tended to rise. In a test employing hydrazine, the pressure loss tended not to rise. In a test employing the test solutions of integrated chemical effect tests, the use of wet rock wool rapidly produced an increase in pressure loss.

Tests were also conducted in sodium tetraborate solution, hydrazine solution, and a solution of hydrochloric acid added to pure water under BWR conditions in integrated chemical effect tests in an environment simulating the containment vessel of a PWR. The solubilities of Al, Si, Fe, Cu, and the like roughly matched the solubilities as calculated from thermodynamics data of the oxides and hydroxides of the various elements. Changes in pressure loss reflected the various test conditions and were complex.

/123

References

(1) J. Dallman, J. Garcia, M. Klasky, B. Letellier and Kerry Howe, "Integrated Chemical Effects Test Project:Test #1 Data Report", LA-UR-05-0124, 2005
(2) J. H. Park, K. Kasza, B. Fisher, J. Oras, K. Natesan and W. J. Shack, "Chemical Effects Head-Loss Research in Support of Generic Safety Issue 191", NUREG/CR-6913, 2006
(3) Jean Marie MATTEI, Yves ARMAND, Ivan VICENA, Bela SOLTESZ, Jozef BATALIK, Vladimir GUBCO, Marek LISKA, Andrea KLEMENTOVA, "Risk of Sump Plugging Experimental program on chemical effects", EUROSAFE 2005
(4) "Fiscal 2006 Test Report on PWR Sump Screen Clogging Incidents. 07 Kishi Report-0004, Japan Nuclear Energy Safety Organization, IAI, 2007.

A. pH-solubility curves of oxides

The following are pH-solubility curves of hydroxides and oxides at 25ºC, considered necessary throughout the study. The crystals of aluminum hydroxide were in the form of Gibbsite and were stable at room temperature. At about 90ºC, they formed Boehmite. In the U.S. test, ICET, the possibility of the presence of amorphous aluminum hydroxide was also pointed out. In the same manner as aluminum hydroxide, silica (SiO_2) was accounted for in crystalline (quartz) and amorphous forms. Iron oxide was calculated as thermodynamically stable hematite (Fe_2O_3), but Goethite (FeO(OH)) was also observed at room temperature. The thermodynamic data and calculation methods employed were as given below. K_i is the equilibrium constant of the various equations.

A.1 Aluminum hydroxide (Gibbsite, $Al(OH)_3$)

. $Al(OH)_3 + 3H^+ = Al^{3+} + 3H_2O$

$\log K_0 = 8.392$

$\log[Al^{3+}] = 8.392 - 3pH$ (1)

· $Al^{3+} + H_2O = AlOH^{+2} + H^+$

$\log K_1 = -5.729$

$\log[AlOH^{2+}] = 2.663 - 2pH$ (2)

· $Al^{3+} + 2H_2O = Al(OH)_2^+ + 2H^+$

$\log K_2 = -11.678$

$\log[Al(OH)_2^+] = -3.286 - pH$ (3)

· $Al^{3+} + 3H_2O = Al(OH)_3 + 3H^+$

$\log K_3 = -17.795$

$\log[Al(OH)_3] = -9.403$ (4)

· $Al^{3+} + 4H_2O = Al(OH)_4^- + 4H^+$

$\log K_4 = -23.595$

$\log[Al(OH)_4^-] = -15.203 + pH$ (5)

The various concentrations were calculated and added using (1) to (5) above to obtain the solubilities. The calculation results are given in Fig. A.1. The red line is the solubility.

A.2 Aluminum hydroxide (amorphous, $Al(OH)_3$)

The thermodynamic data recorded in HSC Chemistry 6.1[(A1)] were employed.

. $Al(OH)_3 + 3H^+ = Al^{3+} + 3H_2O$

$\log K_0 = 11.318$

$\log[Al^{3+}] = 11.318 - 3pH$ (1)

· $Al^{3+} + H_2O = AlOH^{+2} + H^+$

$\log K_1 = -5.729$

$\log[AlOH^{2+}] = 5.589 - 2pH$ (2)

· $Al^{3+} + 2H_2O = Al(OH)_2^+ + 2H^+$

$\log K_2 = -11.678$

$\log[Al(OH)_2^+] = -0.63 - pH$ (3)

· $Al^{3+} + 3H_2O = Al(OH)_3 + 3H^+$

$\log K_3 = -17.795$

$\log[Al(OH)_3] = -6.477$ (4)

/125

· $Al^{3+} + 4H_2O = Al(OH)_4^- + 4H^+$

$\log K_4 = -23.595$

$\log[Al(OH)_4^-] = -12.277 + pH$ (5)

The various concentrations were calculated and added using (1) to (5) above to obtain the solubilities. The calculation results are given in Fig. A.2. The red line is the solubility.

A.3 Quartz (SiO_2)

The thermodynamic data recorded in HSC Chemistry 6.1[(A1)] were employed.

$\log K_4 = -4.000$

$\log[Si(OH)_4] = -4.000$ (1)

· $Si(OH)_4 = SiO(OH)_3^- + H^+$

$\log K_5 = -9.811$

$\log[SiO(OH)_3^-] = -13.811 + pH$ (2)

· $Si(OH)_4 = SiO_2(OH)_2^{2-} + 2H^+$

$\log K_6 = -23.143$

$\log[SiO_2(OH)_2^{2-}] = -27.143 + 2pH$ (3)

· $Si(OH)_4 = SiO_3(OH)^{3-} + 3H^+$

$\log K_7 = -32.822$

$\log[SiO_3(OH)^{3-}] = -36.822 + 3pH$ (4)

· $Si(OH)_4 = SiO_4^{4-} + 4H^+$

$\log K_8 = -49.197$

$\log[SiO_4^{4-}] = -53.197 + 4pH$ (5)

The various concentrations were calculated and added using (1) to (5) above to obtain the solubilities. The calculation results are given in Fig. A.3. The red line is the solubility.

A.4 Amorphous silica (Amorphous, SiO_2)

The thermodynamic data recorded in Table 14.3 of Reference A2 were employed.

$\log K_4 = -2.7136$

$\log[Si(OH)_4] = -2.7136$ (1)

$\cdot SiO_2 + 3H_2O = Si(OH)_3^- + H^+$

$\log K_5 = -12.5368$

$\log[SiO(OH)_3^-] = -12.5368 + pH$ (2)

The various concentrations were calculated and added using (1) and (2) above to obtain the solubilities. The calculation results are given in Fig. A.4. The red line is the solubility.

A.5 Iron oxide (Hematite, Fe_2O_3)

The thermodynamic data recorded in Table 14.3 of Reference A2 were employed.

$\log K_0 = 0.14706$

$\log[Fe^{3+}] = 0.14706 - 3pH$ (1)

$\cdot (1/2)Fe_2O_3 + 2H^+ = Fe(OH)^{2+} + (1/2)H_2O$

$\log K_1 = -2.0660$

/126

$\log[Fe(OH)^{2+}] = -2.0660 - 2pH$ (2)

$\cdot (1/2)Fe_2O_3 + (3/2)H_2O = Fe(OH)_3$

$\log K_3 = -11.3659$

$\log[Fe(OH)_3] = -11.3659$ (3)

$\cdot (1/2)Fe_2O_3 + (5/2)H_2O = Fe(OH)_4^- + H^+$

$\log K_3 = -20.9669$

$\log[Fe(OH)_4^-] = -20.9669 + pH$ (4)

The various concentrations were calculated and added using (1) to (4) above to obtain the solubilities. The calculation results are given in Fig. A.4. The red line is the solubility.

A.6 Copper oxide (CuO)

$\log K_0 = 7.6749$

$\log[Cu^{2+}] = 7.6749 - 2pH$ (1)

$\cdot CuO + H^+ = Cu(OH)^+$

$\log K_1 = -2.1568$

$\log[Cu(OH)^+] = -2.1568 - pH$ (2)

$\cdot CuO + H_2O = Cu(OH)_2$

$\log K_2 = -8.6620$

$\log[Cu(OH)_2] = -8.6620$ (3)

$\cdot CuO + 2H_2O = Cu(OH)_3^- + H^+$

$\log K_3 = -18.04298$

$\log[Cu(OH)_3^-] = -18.04298 + pH$ (4)

$\cdot CuO + 3H_2O = Cu(OH)_4^{2-} + 2H^+$

$\log K_4 = -31.6701$

$\log[Cu(OH)_4^{2-}] = -31.6701 + 2pH$ (5)

The various concentrations were calculated and added using (1) to (5) above to obtain the solubilities. The calculation results are given in Fig. A.5. The red line is the solubility.

A.7 Zinc oxide (ZnO)

The thermodynamic data recorded in Table 14.3 of Reference A2 were employed.

$\log[Zn^{2++}] = 11.1690 - 2pH$ (1)

$\cdot ZnO + H^{+} = Zn(OH)^{+}$

$\log K_1 = 2.4075$

$\log[Zn(OH)^{+}] = 2.4075 - pH$ (2)

$\cdot ZnO + H_2O = Zn(OH)_2$

$\log K_2 = -7.8506$

$\log[Zn(OH)_2] = -7.8506$ (3)

$\cdot ZnO + 2H_2O = Zn(OH)_3^{-} + H^{+}$

$\log K_3 = -16.9340$

/127

$\log[Zn(OH)_3^{-}] = -16.9340 + pH$ (4)

The various concentrations were calculated and added using (1) to (4) above to obtain the solubilities. The calculation results are given in Fig. A.6. The red line denotes solubility.

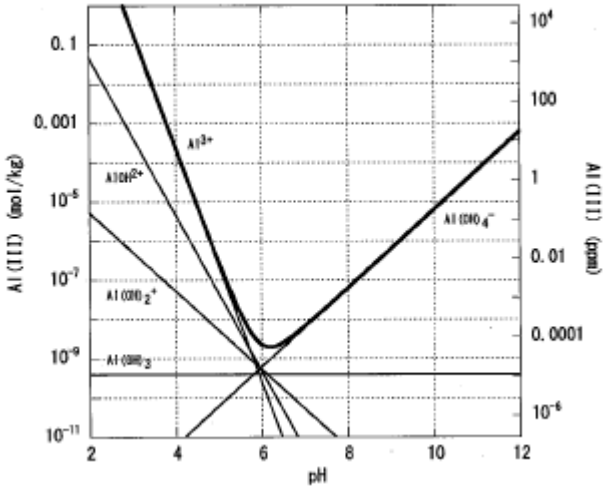

Fig. A.1 pH-solubility curve of aluminum hydroxide (Gibbsite, $Al(OH)_3$)

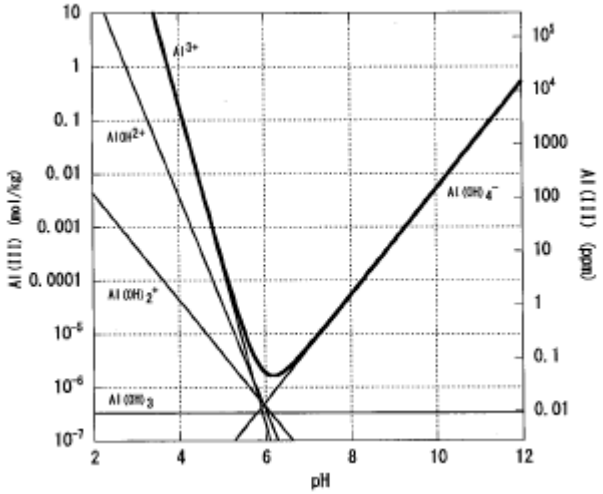

Fig. A.2 pH-solubility curve of aluminum hydroxide (Amorphous, $Al(OH)_3$)

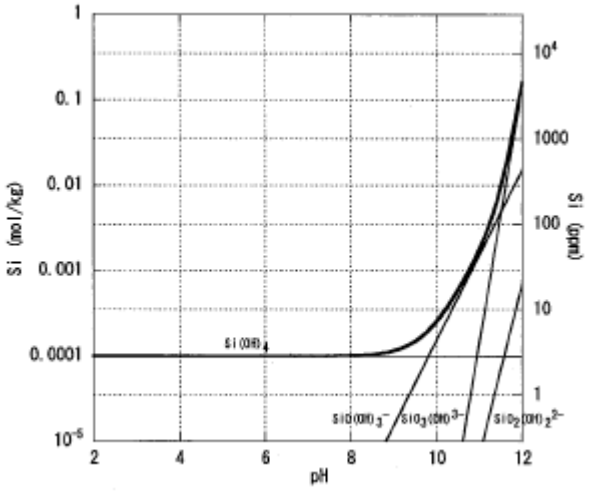

Fig. A.3 pH-solubility curve of quartz (SiO_2)

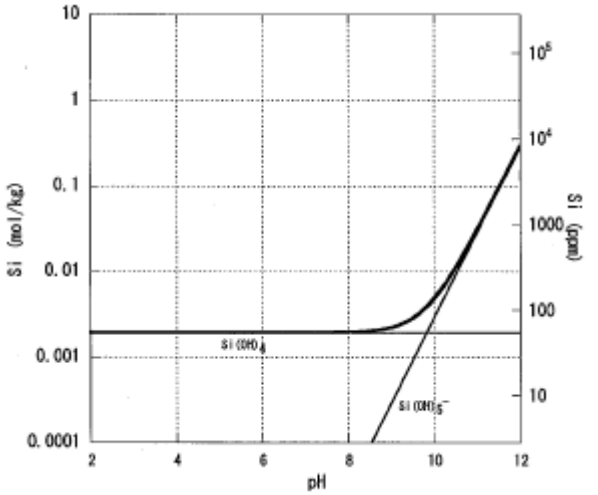

Fig. A.4 pH-solubility curve of amorphous silica (Amorphous, SiO_2)

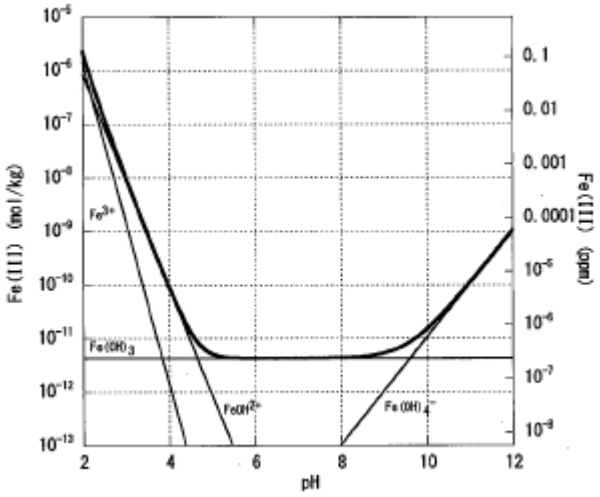

Fig. A.5 pH-solubility curve of iron oxide (Hematite, Fe_2O_3)

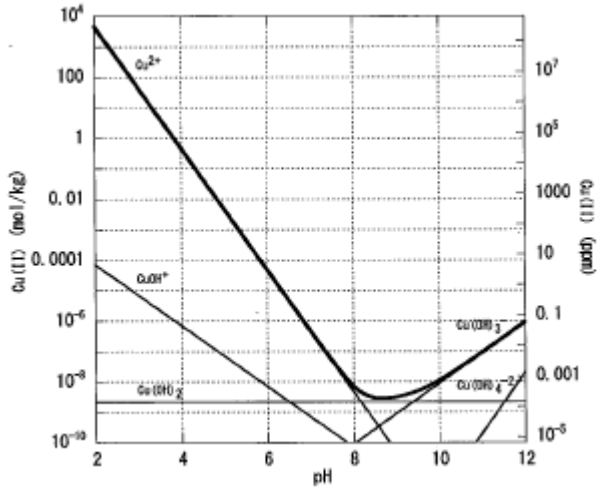

Fig. A.6 pH-solubility curve of copper oxide (CuO)

/131

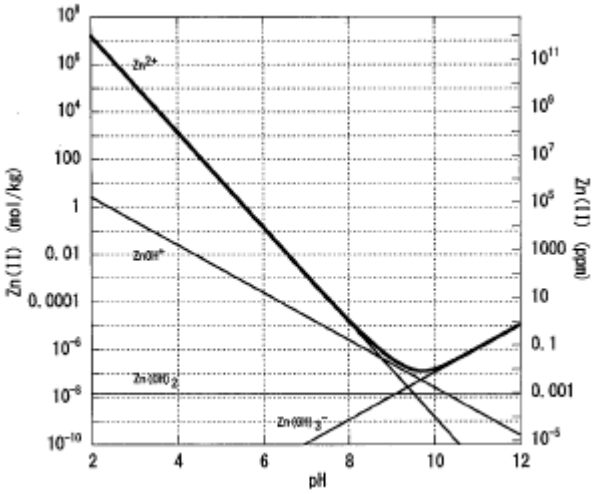

Fig. A.7 pH-solubility curve of zinc oxide (ZnO)

References

A1. HSC Chemistry 6.1, Outokumpu Research Oy.

A2. D. A. Palmer, R. Fernandez-Prini and A. H. Harvey (Eds.), *Aqueous System at Elevated Temperatures and Pressures: Physical Chemistry in Water, Steam and Hydrothermal Solutions*, Elsevier, 2004

/last

JNES
Safety Standard Division
Japan Nuclear Energy Safety Organization, AIA

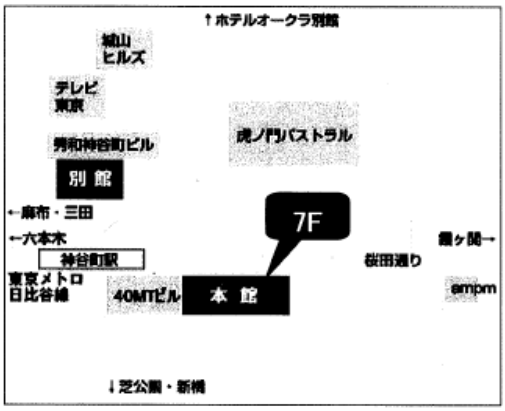

[Rough map of Toranomon location of JNES in Tokyo]

Safety Standards Division

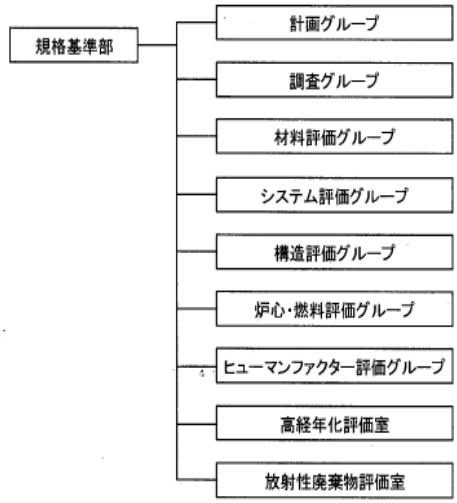

Planning Group
Investigation Group
Materials Evaluation Group
System Evaluation Group
Structural Evaluation Group
Reactor Core and Fuel Evaluation Group
Human Factor Evaluation Group
Aging Evaluation Group
Radioactive Waste Evaluation Group

Postal code 105-0001
TOKYU REIT Toranomon Bldg. 7F, 3-17-1 Toranomon, Minato-ku, Tokyo
Safety Standards Representative Tel: 03-4511-1702
Safety Standards Representative Fax: 03-4511-1898
Safety Standards Representative E-mail: SSD@jnes.go.jp